Nonlocal electrodynamics in Weyl semimetals

B. Rosenstein,[1,2] H. C. Kao,[3,*] and M. Lewkowicz[2]
[1]*Electrophysics Department, National Chiao Tung University, Hsinchu 30050, Taiwan, Republic of China*
[2]*Physics Department, Ariel University, Ariel*
[3]*Physics Department, National Taiwan Normal University, Taipei 11677, Taiwan, Republic of China*
(Received 19 August 2015; revised manuscript received 8 February 2017; published 28 February 2017)

Recently synthesized three-dimensional materials with Dirac spectrum exhibit peculiar electric transport qualitatively different from its two-dimensional analog, graphene. By neglecting impurity scattering, the real part of the conductivity is strongly frequency dependent, while the imaginary part is nonzero unlike in undoped, clean graphene. The Coulomb interaction between electrons is unscreened as in a dielectric and hence is long range. We demonstrate that the interaction correction renders the electrodynamics nonlocal on a mesoscopic scale. The longitudinal conductivity $\sigma_{\rm L}$ and the transverse conductivity $\sigma_{\rm T}$ are different in the long-wavelength limit and consequently the standard local Ohm's law description does not apply. This leads to several remarkable effects in optical response. The p-polarized light generates in these materials bulk plasmons as well as the transversal waves. At a specific frequency the two modes coincide, a phenomenon impossible in a local medium. For any frequency there is a Brewster angle where total absorption occurs, turning the Weyl semimetals opaque. The effect of the surface, including the Fermi arcs, is discussed.

DOI: 10.1103/PhysRevB.95.085148

I. INTRODUCTION

One of the common assumptions of electrodynamics in media is that the effect of external electric fields can be described *locally* by constitutive relations connecting the "induced" currents to the electric field even when spatial dispersion is present. Because of space-time translational symmetry of the material, the relation between the Fourier components reads

$$J_i(\omega,\mathbf{k}) = \sigma_{ij}(\omega,\mathbf{k})E_j(\omega,\mathbf{k}), \tag{1}$$

within linear response. Here σ_{ij} is the ac conductivity tensor with indices $i,j = x,y,z$, and $\omega,\mathbf{k}$ the frequency and wave number. With rotational, reflection, and time-reversal invariance, the conductivity tensor can be uniquely decomposed into the transversal and longitudinal parts [1]:

$$\sigma_{ij}(\omega,\mathbf{k}) = \left(\delta_{ij} - \frac{k_i k_j}{k^2}\right)\sigma_{\rm T}(\omega,\mathbf{k}) + \frac{k_i k_j}{k^2}\sigma_{\rm L}(\omega,\mathbf{k}). \tag{2}$$

Locality of the electrodynamic response means that the long-wavelength limit exists. In such limit, δ_{ij} is the only second-rank tensor consistent with the symmetries of the system, and hence the conductivity tensor simplifies into

$$\sigma_{ij}(\omega,\mathbf{k}=\mathbf{0}) \equiv \sigma_{ij}(\omega) = \delta_{ij}\sigma(\omega). \tag{3}$$

Although locality seems to be ubiquitous in condensed matter systems, it is not guaranteed on the microscopic level [1]. Ohm's law is generally applicable in all ordinary conductors, including disordered metal, semimetals at arbitrary temperature, and semiconductors at nonzero temperature. If disorder is significant, one has usual Drude transport with a mean free path even at zero temperature providing the necessary length scale to ensure the locality, Eq. (3). Even in clean metals at zero temperature, the *noninteracting* electron gas (or Landau liquid for short-range interactions) is local. This is not evident since there is no energy gap, so there are gapless charged excitations. The standard "Lindhard" type calculations [1] in an absolutely clean metal show that $\sigma_{\rm T}$ and $\sigma_{\rm L}$ are not independent at small wave vectors,

$$\begin{aligned}\sigma_{\rm T}(\omega,\mathbf{k}=\mathbf{0}) &= \sigma_{\rm L}(\omega,\mathbf{k}=\mathbf{0}) \equiv \sigma(\omega);\\ \sigma_{\rm L}(\omega,\mathbf{k}) - \sigma_{\rm T}(\omega,\mathbf{k}) &= \beta(\omega)k^2 + O\left(k^4\right),\end{aligned} \tag{4}$$

thus leading to the local Ohm's law equation (3).

It was shown [2] that all the above reasons ensuring locality are inapplicable to clean graphene at Dirac point when Coulomb interactions are included. The reason for the nonlocality is that the Coulomb interactions remain unscreened and thus long range. The question arises if this is also true for the recently discovered three-dimensional (3D) Weyl semimetals (WSMs).

Although it has been known for a long time that the two-band electronic structure of bismuth may be described by a four-component nearly 3D massless Dirac fermion [3], only recently was possible physical realization predicted [4,5]. Since then, several materials have been discovered: the time-reversal invariant topological Dirac semimetal Na_3Bi [6–8], a bulk crystal symmetry protected semimetal Cd_3As_2 with a single pair of Dirac points [9–11], and crystals on the phase transition boundary between topological and band insulators HgCdTe [12]. Moreover [13–16], WSMs such as TaAs were found to exhibit Fermi arcs on their surface [4]. All these materials exhibit a great variety of new electromagnetic transport and optical phenomena [not seen in a two-dimensional (2D) WSM-like graphene] including giant diamagnetism, quantum magnetoresistance showing linear field dependence [17–20], superconductivity [21], etc.

In this paper we assume that the WSM is clean enough, so that the disorder scale is irrelevant and the chemical potential is tuned to the Dirac point. When the interaction is neglected, the ac conductivity of a WSM remains local as expected [22,23]. However, by calculating the screening due to the interaction corrections [22,24,25], it becomes clear that the Coulomb

*Corresponding author: hckao@ntnu.edu.tw

interaction is still long range unlike in metals. Hence, there is no good reason to insist that the electric response in a WSM is still local. In fact, we demonstrate by explicit calculation of the interaction effects using a rather generic model of WSMs that the electrodynamics is indeed nonlocal. The rather unusual macroscopic electrodynamics then is formulated and applied to analyze various optical phenomena in which the nonlocality can be demonstrated. The optical generation of both longitudinal (plasmon) and transversal waves and their subsequent propagation in the material are considered. The effects of the surface including those due to the Fermi arcs (that depend on the crystallographic orientation of the surface) are studied using a microscopic model defined next.

II. ac LINEAR RESPONSE OF THE BULK WEYL SEMIMETAL

A. The model

An analogous calculation in graphene [2,26] reveals that in order to avoid complications linked to the absence of scale separation in systems with relativistic massless fermions, one should use a well-defined lattice model. Electrons in a WSM may be described accurately enough by the tight-binding model of nearest neighbors on a cubic lattice [22,27] $\mathbf{n} = n_i \mathbf{a}_i$, having space-inversion and time-reversal symmetries, and translational symmetry for the unlimited bulk.

The noninteracting Hamiltonian is

$$\hat{K} = \frac{i\gamma}{2} \sum_{n,i} c_{\mathbf{n}}^{\sigma\dagger} \sigma_i^{\sigma\rho} c_{\mathbf{n}+\mathbf{a}_i}^{\rho} + \text{H.c.}, \tag{5}$$

where $c_{\mathbf{n}}^{\sigma\dagger}$ are the creation operators with spin $\sigma = 1,2$, γ the hopping energy, and σ_i are the Pauli matrices. The Fermi velocity is $v = \gamma a/\hbar$ and a the lattice spacing. One observes eight Weyl points inside the Brillouin zone (BZ). Four are right handed: one in the center (the Γ point) and three on the faces (X); while four are left handed: three on the edges (M) and one in the corner (R).

In terms of Fourier components, the Coulomb interaction takes the form

$$\widehat{V} = \frac{\alpha}{2\mathcal{V}} \sum_{\mathbf{pkl}} v_{\mathbf{p}} c_{\mathbf{k}+\mathbf{p}}^{\sigma\dagger} c_{\mathbf{k}}^{\sigma} c_{\mathbf{l}-\mathbf{p}}^{\rho\dagger} c_{\mathbf{l}}^{\rho}, \tag{6}$$

where $\alpha = \frac{e^2}{\epsilon\hbar v}$ is the coupling with ϵ being the dielectric constant of the WSM. $\mathcal{V}$ is the sample volume and

$$v_{\mathbf{p}} = \frac{\pi}{\sin^2(p_x a/2) + \sin^2(p_y a/2) + \sin^2(p_z a/2)}. \tag{7}$$

One may extract σ_{T} and σ_{L} from Eq. (2): $k_i k_j \sigma_{ij}/k^2 = \sigma_{\mathrm{L}}$ and $\sigma_{ii} = 2\sigma_{\mathrm{T}} + \sigma_{\mathrm{L}}$ (where the summation convention was used). In particular, leading interaction corrections are given by the vertex renormalization, self-energy, and glasses diagrams, respectively. Details involving Matsubara action and Feynmann rules appear in Appendix A.

B. The electrodynamics of a free Fermi gas is local

The free conductivity tensor at Dirac point is

$$\sigma_{ij}(\omega,\mathbf{k}) = \frac{N}{24\pi\omega}\frac{e^2}{\hbar v}\left(1 - \frac{i}{\pi}\log\frac{\Omega^2}{\omega^2 - v^2k^2}\right) \times \{\delta_{ij}(\omega^2 - v^2k^2) + v^2 k_i k_j\}. \tag{8}$$

N is the number of Weyl fermions and $\Omega \simeq 2.5\pi v/a$ is the ultraviolet frequency cutoff of order 10^{15} s^{-1}. For the details of the calculation see Appendix B.

In the long-wavelength limit one recovers the ac conductivity $\sigma_{ij}^0(\omega,\mathbf{k}=\mathbf{0}) = \sigma_0(\omega)\delta_{ij}$ with

$$\sigma_0(\omega) = \frac{N\omega}{24\pi}\frac{e^2}{\hbar v}\left(1 - \frac{i}{\pi}\log\frac{\Omega^2}{\omega^2}\right). \tag{9}$$

It has an imaginary part, logarithmically divergent as a function of Ω/ω. Thus the dc conductivity is zero, i.e., the material behaves like an insulator, qualitatively different from graphene. It is well known that in 3D Weyl semimetals the Coulomb interaction is unscreened [22,24,28]. The dependence on the wave vector follows uniquely from the pseudorelativistic invariance of the free Weyl gas [2]. From Eq. (4), we deduce

$$\beta^0(\omega) = -\sigma_0(\omega)v^2/\omega^2. \tag{10}$$

C. Electron-electron interactions cause nonlocality of electrodynamics

Using the Coulomb interaction in Eq. (6), one obtains the corrections to first order in (renormalized) coupling. While the corrections to σ_{T} and σ_{L} are small, the correction to the difference $\sigma_{\mathrm{nl}} \equiv \sigma_{\mathrm{L}} - \sigma_{\mathrm{T}}$ can be considerable in the homogeneous regime $v^2k^2 \ll \omega^2$. In particular, for $\mathbf{k} = 0$ the real and imaginary parts of σ_{nl} for $N \gg 1$ Weyl nodes are

$$\frac{\sigma'_{\mathrm{nl}}}{\omega} = -\frac{e^2\alpha}{\hbar v}\frac{N^2}{48\pi^2}\log\left(\frac{\Omega^2}{\omega^2}\right), \qquad \frac{\sigma''_{\mathrm{nl}}}{\omega} = -\frac{e^2\alpha}{\hbar v}\frac{N^2}{96\pi^3}\log^2\left(\frac{\Omega^2}{\omega^2}\right). \tag{11}$$

One observes that the signs of both are negative. Details of the calculation of both σ_{T} and σ_{L} and expression for arbitrary N are given in Appendix C.

III. FERMI ARCS CONTRIBUTION TO SURFACE CONDUCTIVITY

In the absence of topological surface states the conductivity changes abruptly from the vacuum to the bulk value, Eq. (9). However, cutting the crystal along a certain crystallographic axis such as [110] [Fig. 1(b)] causes Fermi arcs, albeit, a cut along [100], for example, is topologically trivial, as is shown in Appendix D.

Edge states along the diagonal cut [110]

The translation invariance along the z direction allows one again to Fourier transform first

$$c_{n_x,n_y,n_z}^{\beta} = \sum_{k_z} e^{ik_z n_z} c_{n_x,n_y,k_z}^{\beta}. \tag{12}$$

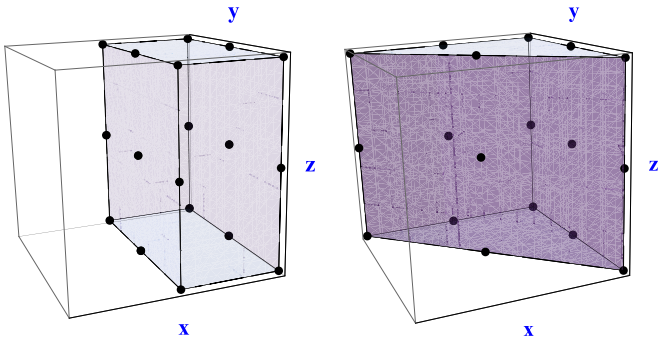

(a) (b)

FIG. 1. A simple tight-binding model of WSM exhibiting Fermi arc. A cubic lattice cut along (in a plane perpendicular to the z axis) (a) the [100] plane and (b) the [110] plane.

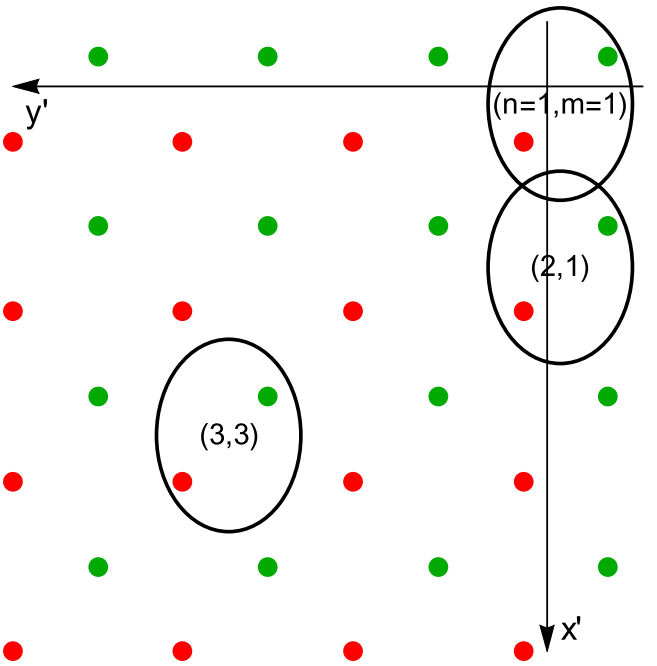

FIG. 2. The cubic WSM lattice (in a plane perpendicular to the z axis) cut along the diagonal [110]. The x and y axes are rotated by 45° to x' and y'. The unit cells [consisting of the two sublattices A (green) and B (red)] are labeled with the integers n and m.

It is convenient to rotate the remaining axes by 45° to x' and y' and label the atoms in a plane perpendicular to z with two integers n and m, and a sublattice index I taking two values A and B (the protuberance of the zigzag surface and the sinkage) (see Fig. 2). The tight-binding model including the surface becomes

$$K=\frac{iv}{2}\sum_n\left\{\begin{array}{l}\sum\limits_{m=2}c^{A\dagger}_{nm}\left(\sigma_x c^B_{nm}+\sigma_y c^B_{n,m-1}\right)+c^{A\dagger}_{n,1}\sigma_x c^B_{n,1}+\sum\limits_{m=1}c^{B\dagger}_{nm}\left(\sigma_x c^A_{n+1,m+1}+\sigma_y c^A_{n+1,m}\right)\\ -\sum\limits_{m=2}\left(c^{B\dagger}_{nm}\sigma_x c^A_{nm}+c^{B\dagger}_{n,m-1}\sigma_y c^A_{nm}\right)-\sum\limits_{m=1}\left(c^{A\dagger}_{n+1,m+1}\sigma_x c^B_{nm}+c^{A\dagger}_{n+1,m}\sigma_y c^B_{nm}\right)-c^{B\dagger}_{n,1}\sigma_x c^A_{n,1}\end{array}\right\}. \tag{13}$$

This can be rearranged as

$$K=\frac{iv}{2}\sum_n\left\{\begin{array}{l}\sum\limits_{m=2}^{M-1}\left\{c^{A\dagger}_{nm}\left(\sigma_x c^B_{nm}-\sigma_x c^B_{n-1,m-1}+\sigma_y c^B_{n,m-1}-\sigma_y c^B_{n-1,m}\right)\right.\\ \quad\left.+c^{B\dagger}_{nm}\left(\sigma_x c^A_{n+1,m+1}-\sigma_x c^A_{nm}+\sigma_y c^A_{n+1,m}-\sigma_y c^A_{n,m+1}\right)\right\}\\ \quad+c^{B\dagger}_{n,1}\left(\sigma_x c^A_{n+1,2}-\sigma_x c^A_{n,1}+\sigma_y c^A_{n+1,1}-\sigma_y c^A_{n,2}\right)+c^{A\dagger}_{n,1}\left(\sigma_x c^B_{n,1}-\sigma_y c^B_{n-1,1}\right)\\ \quad+c^{B\dagger}_{n,M}\left(\sigma_y c^A_{n+1,M}-\sigma_x c^A_{n,M}\right)+c^{A\dagger}_{n,M}\left(\sigma_x c^B_{n,M}-\sigma_x c^B_{n-1,M-1}+\sigma_y c^B_{n,M-1}-\sigma_y c^B_{n-1,M}\right)\end{array}\right\}. \tag{14}$$

Therefore one can perform the Fourier transform over n:

$$c^{I\alpha}_{nm}=\sum_k e^{-i\sqrt{2}nk}c^{I\alpha}_{km}. \tag{15}$$

For fixed k,k_z the part of the Hamiltonian becomes

$$K_{k,k_z}=\frac{iv}{2}\left\{\begin{array}{l}\sum\limits_{m=2}^{M-1}\left\{c^{A\dagger}_m\left(h_{m,m}c^B_m+h_{m,m-1}c^B_{m-1}\right)+c^{B\dagger}_m\left(h^\dagger_{m,m+1}c^A_{m+1}+h^\dagger_{m,m}c^A_m\right)\right\}\\ \quad+c^{A\dagger}_1 h_{11}c^B_1+c^{B\dagger}_1\left(h^\dagger_{12}c^A_2+h^\dagger_{11}c^A_1\right)+c^{A\dagger}_M\left(h_{MM}c^B_M+h_{M,M-1}c^B_{M-1}\right)+c^{B\dagger}_M h^\dagger_{MM}c^A_M\end{array}\right\}, \tag{16}$$

where

$$\begin{aligned}h_{mm}=h_{11}=h_{MM}&=\sigma_x-e^{i\sqrt{2}k}\sigma_y;\\ h_{m,m-1}=h_{M,M-1}&=\sigma_y-e^{i\sqrt{2}k}\sigma_x.\end{aligned} \tag{17}$$

The Schrödinger equations away from the surface are

$$\begin{aligned}\frac{iv}{2}\left\{\sigma_x\psi^B_m+\sigma_y\psi^B_{m-1}-e^{i\sqrt{2}k}\left(\sigma_x\psi^B_{m-1}+\sigma_y\psi^B_m\right)\right\}&=E\psi^A_m,\\ \frac{iv}{2}\left\{e^{-i\sqrt{2}k}\left(\sigma_x\psi^A_{m+1}+\sigma_y\psi^A_m\right)-\left(\sigma_x\psi^A_m+\sigma_y\psi^A_{m+1}\right)\right\}&=E\psi^B_m.\end{aligned} \tag{18}$$

The edge states obey the condition $\psi^A_{m+1} = \lambda\sigma_z\psi^A_m$ and the Schrödinger equation $h^\dagger\psi^B = h\psi^A = 0$, where

$$h = \sigma_x(\lambda\sigma_z e^{-i\sqrt{2}k} - 1) + \sigma_y(e^{-i\sqrt{2}k} - \lambda\sigma_z), \tag{19}$$

which results in

$$\lambda = i\frac{1 - ie^{-i\sqrt{2}k}}{1 + ie^{-i\sqrt{2}k}}. \tag{20}$$

The effective theory on the surface is

$$H_{\rm arc} = \frac{i}{2}\sum_{n,n_z} c^\dagger_{n,n_z}\sigma_z c_{n,n_z+1} + \text{H.c.}$$
$$= \frac{1}{(2\pi)^2}\int_{k_z=-\pi}^{\pi}\int_{k=-\pi/\sqrt{2}}^{\pi/\sqrt{2}} c^\dagger_{k,k_z}k_z\sigma_z c_{k,k_z}. \tag{21}$$

The dispersion in the z direction is therefore $E(k_z) = \pm\frac{i}{2}(e^{ik_z} - e^{-ik_z}) = \mp\sin k_z$. The 2D conductivity tensor of this one-dimensional system therefore acquires only the imaginary component [29]

$$\sigma_{zz} = -ic\frac{\omega_{fa}}{\omega}, \tag{22}$$

with the characteristic frequency $\omega_{fa} \equiv \sqrt{2}\frac{e^2\gamma}{c\hbar^2}$ in the terahertz range.

The cubic WSM lattice (in a plane perpendicular to the z axis) cut along the diagonal [110]. The x and y axes are rotated by 45° to x' and y'. The unit cells [consisting of the two sublattices A (green) and B (red)] are labeled with the integers n and m.

IV. OPTICS/PLASMONICS WITHIN A WSM

A. Coexistence of transversal and longitudinal waves in WSM

Employing the macroscopic Maxwell equations [30,31], we now investigate the behavior of electromagnetic waves in a WSM. By combining Ampère's and Faraday's law, we find the following two modes: (i) **E** transversal:

$$1 + i\frac{4\pi}{\omega}\sigma_{\rm T}(\omega,\mathbf{p}) = \frac{c^2p^2}{\omega^2}. \tag{23}$$

(ii) **E** longitudinal:

$$1 + i\frac{4\pi}{\omega}\sigma_{\rm L}(\omega,\mathbf{q}) = 0. \tag{24}$$

Note that when $\omega \ll \Omega$ the imaginary part of the conductivity in Eq. (9) is dominant. Thus, the dispersion relations and for the transversal and longitudinal modes are (see Appendix E for details and full expressions for arbitrary N)

$$p = \frac{\omega}{c}\sqrt{\frac{Ne^2}{6\pi v\hbar}\log\frac{\Omega^2}{\omega^2}};$$
$$q = \frac{\omega}{v}\sqrt{1 - \frac{N\alpha}{4\pi}\log\frac{\Omega^2}{\omega^2}}, \tag{25}$$

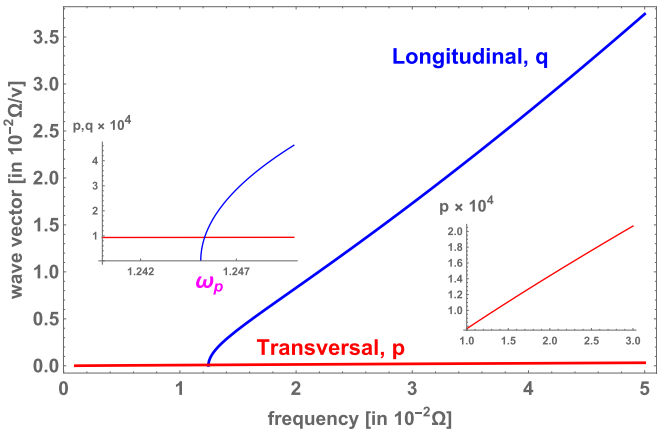

FIG. 3. Two branches of excitations in neutral plasma of the WSM: the transverse (red) and longitudinal (blue) wave vectors. Both are monotonically increasing as a function of frequency (the inset on the right is for the transverse wave). At the intersection point the electromagnetic wave is monochromatic (the left inset).

respectively. The real part of the conductivity determines the penetration depth

$$\delta_{\rm T} = \frac{12\hbar v}{Ne^2\omega^2}c^2p;$$
$$\delta_{\rm L} = \frac{v^2}{\omega^2}\frac{4\pi}{N\alpha}q. \tag{26}$$

We present the results for p,q in units of Ω/v as functions of ω/Ω in Fig. 3. Here, $N = 4$, $v = c/300$, $\epsilon = 5.5$, and $\Omega \simeq 2.5\pi v/a = 10^{15}$ s^{-1} (characteristic of Na_3Bi and Cd_3As_2). Since the light wave vector **p** is real for all frequencies $\omega < \Omega$, it is nondissipating (see the right inset in Fig. 3). In contrast, the longitudinal wave vector **q** is real only for frequencies above the threshold ω_p, given by

$$\omega_p = \Omega\exp\left\{-\frac{1}{N\alpha}[(\pi - \alpha) + \sqrt{6\pi^2/\epsilon + (\pi - \alpha)^2}]\right\}. \tag{27}$$

Here ω_p, the "plasma frequency" (in the terahertz range), is that of a neutral plasma rather than that of the charged plasma in metals.

By taking the difference between Eqs. (23) and (24), one obtains

$$i\frac{4\pi}{\omega}\sigma_{\rm nl}(\omega,\mathbf{k}) = -\frac{c^2k^2}{\omega^2}. \tag{28}$$

This leads to $4\pi i\omega\beta_0(\omega) = c^2$ upon using Eq. (10). In local materials, this generally cannot be satisfied. In a WSM, however, $\sigma_{\rm nl}(\omega,\mathbf{0})$ is finite and such solutions do exist and can be seen in Fig. 3 (the left inset). Therefore at this special value of the wave vector both transverse and longitudinal waves exist.

B. Additional boundary condition

To observe the effect of nonlocality, let us consider the reflection and transmission of an incident electromagnetic wave on a vacuum-WSM interface. To simplify, we will choose the xz plane to be the incident one. For p-polarized incoming

waves,

$$\frac{\mathbf{E}^{\rm vac}}{E_0} = \left\{\frac{k_z}{k},0,\frac{-k_x}{k}\right\}e^{i(k_x x+k_z z)} - r\left\{\frac{k_z}{k},0,\frac{k_x}{k}\right\}e^{i(k_x x-k_z z)}, \tag{29}$$

where E_0 is the incoming amplitude and r the reflection coefficient with $k_x > 0$ and $k_z < 0$ and θ the incident angle. The field in the WSM is given by

$$\frac{\mathbf{E}^{\rm WSM}}{E_0} = t_{\rm T}\left\{\frac{p_z}{p},0,\frac{-k_x}{p}\right\}e^{i(k_x x+p_z z)} + t_{\rm L}\left\{\frac{k_x}{q},0,\frac{q_z}{q}\right\}e^{i(k_x x+q_z z)}, \tag{30}$$

where $t_{\rm T}$ and $t_{\rm L}$ are the transmitted transversal and longitudinal amplitudes.

The previous formulation may also be used to analyze the problems like in exciton physics [31,32]. In addition to the usual four boundary conditions, one also needs the so-called additional boundary condition (ABC), since there are two different modes propagating in the bulk [32,33]. With a "sharp" interface no current may escape the WSM, and the ABC becomes $\sigma_{zx}E_x^{\rm WSM} + \sigma_{zz}E_z^{\rm WSM} = 0$. Applying all these boundary conditions, we obtain the following reflection and transmission amplitudes:

$$r = \frac{1-D}{1+D};\quad t_{\rm T} = \frac{2k/p}{1+D};\quad t_{\rm L} = -\frac{2k_x q(p^2-k^2)}{kq_z p^2(1+D)};$$
$$D = \frac{k^2 p_z q_z - (p^2-k^2)k_x^2}{k_z q_z p^2}. \tag{31}$$

Remarkably, $D = 1$ at certain frequency-dependent incident angles and the WSM becomes opaque.

In contrast, the s-polarized wave does not generate a longitudinal wave. Hence, the amplitudes are standard. In Fig. 4 the amplitudes for the p polarizations and s polarizations are presented. It shows the vanishing of the p-polarization reflection coefficient at an incident angle in the terahertz range. In Fig. 5, the (p) reflection amplitude as a function of frequency for various incident angles is shown.

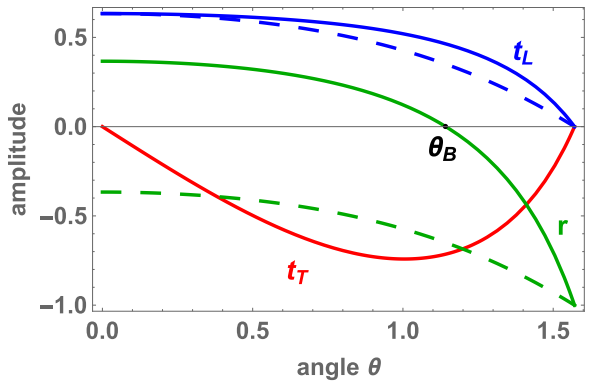

FIG. 4. Reflection and transmission amplitudes as a function of θ. The p-polarization amplitudes (solid): reflected (green), transmitted transversal (red), and longitudinal (blue); the incident radiation is totally absorbed by the WSM at Brewster's angle θ_B. The s-polarization amplitudes are plotted dashed.

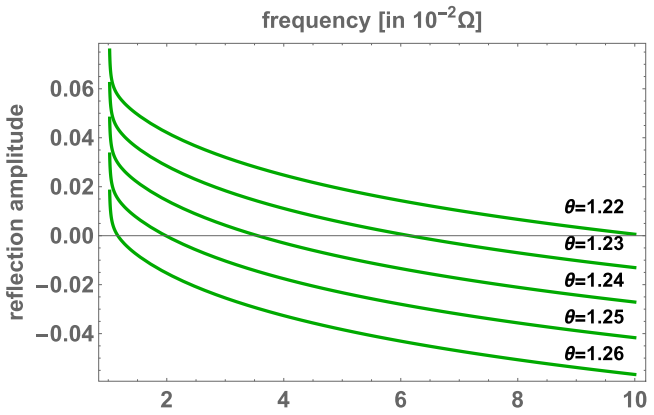

FIG. 5. The (p) reflection amplitude r as a function of frequency for various incident angles displaying the total absorption.

C. Effect of Fermi arcs on optics

The contribution of the Fermi arc is obtained in a standard way [34] and no ABC is needed. Now the optical response is highly anisotropic, leading for $\omega \ll \omega_{fa}$ to large polarization effects. In particular, for the incident wave vector in the xz plane, the p-polarized light is not affected. Therefore the effects of nonlocality in the p-polarized light, Eq. (31), are present without correction. On the contrary, the reflection/transmission amplitudes of the boundary for the s polarization are

$$r_{\rm arc} = -\frac{1}{1+i\frac{2ck_z}{\omega_{fa}}};\quad t_{\rm arc} = \frac{1}{1-i\frac{\omega_{fa}}{2ck_z}}. \tag{32}$$

V. DISCUSSION

The calculation of the leading Coulomb interaction effect in a type I 3D WSM reveals that its macroscopic electrodynamics becomes nonlocal as the ac conductivity tensor becomes nonanalytic at small wave vectors. As a result, the longitudinal and the transversal conductivities, $\sigma_{\rm L}$ and $\sigma_{\rm T}$, become different and consequently the standard local Ohm's law no longer applies. The origin of the nonlocality is a unique combination of the long-range Coulomb interaction and the linear dispersion relation of the quasiparticles. The optical response of a WSM is sensitive to the nonlocality effect.

The most remarkable distinct feature is the splitting of the incident p-polarized light into a transversal and a longitudinal wave. A local medium such as a dielectric or a metal does not allow the coexistence of the two modes. In a dielectric there are no plasmons, while in a metal the transversal waves do not propagate. We find that for parameters typical for materials like TaAs the effect is observable in the terahertz range. The two modes coincide at a specific frequency. The effect of total absorption of the p-polarized wave in WSM is similar to that in the "usual" "Brewster's angle" of a dielectric material. However, the frequency dependence differs drastically. It originates from the fact that the transmitted wave consists of a transversal and a longitudinal wave, causing the WSM Brewster's angle to depend on the plasmon wave number.

The effect of nonlocality is easily distinguished from the much more evident effect of the Fermi arcs on the surface of the WSM. The latter depends sensitively on the direction of

the surface with respect to the crystallographic axes. For some surfaces (see our example of the [100] for our simple tight-binding model) the arcs are avoided even for well separated Weyl points. For more generic edges like [110] Fermi arcs appear and before the light enters the bulk it is reflected by a highly anisotropic surface layer that is typically akin to the neutral 2D "regular" semimetal (parabolic dispersion relation with effective mass m) with $n/m = \sqrt{2}v/\hbar a$, where n is the density of carriers with a peculiarity that the 2D conductivity tensor is a rank-one symmetric matrix (just the σ_{zz} component is nonzero in our explicit example). The reflection of the arc is highly polarization and orientation dependent and has a frequency dependence very different from that of the bulk WSM one. The nonlocal conductivity of Fermi arcs as probed by a magnetic field was investigated in [35,36].

Finally let us mention the limitations of our formulas. The applicability of perturbation theory in 3D WSMs has been recently addressed by several groups who used renormalization group and other nonperturbative methods such as the random phase and large N approximations [25,37,38]. The latter shows perturbation theory to be reliable over a wide range of α up to a critical value $\alpha_c \approx 14$. Typical values of the background dielectric constant in 3D WSMs lies in the range $\epsilon \sim 5$–40 [25,39,40], which assures α below α_c. In contrast, α_c was found to be 0.78 in 2D [41]. This is close to the values measured in the samples substrated on boron nitride or suspended samples [42,43], and therefore perturbation theory is less reliable in such case.

Several unavoidable factors can set limit to the nonlocality phenomenon. The calculation was done at zero temperature, while possible experiment would be performed at finite temperature. The thermal excitations create screening and thus limit the nonlocality range to distances smaller than the thermal screening length. Disorder, similar to puddles in graphene, is also present and the averaging over mean free path will average away the nonlocality. An additional obstacle seen clearly in angle-resolved photoemission spectroscopy images is the chemical potential. WSM away from the neutrality point is a regular low electron (hole) density metal, and therefore is local beyond the screening length. The effect that we have described would be washed away if the wavelength of the electromagnetic wave is longer than such a length scale.

To summarize, our result is applicable as long as $\max[k_B T, \mu, \frac{\hbar}{\tau}] \ll \hbar\omega$, where τ is the relaxation time due to impurities.

ACKNOWLEDGMENTS

We are indebted to W. B. Jian, I. Herbut, E. Farber, C. W. Luo, and D. Cheskis. The work of H.K. and B.R. was supported by NSC of Republic of China Grants No. 101-2112-M-003-002-MY3 and No. 103-2112-M-009-009-MY3.

APPENDIX A: INTERACTION CORRECTIONS TO THE BULK CONDUCTIVITY OF WSM

1. The current density in the tight-binding model

The minimal substitution determines the coupling of the external electromagnetic field, described by vector potential A_i with electrons on the lattice:

$$\widehat{K}_{mc}[A(r,t)] = \frac{i}{2}\sum_{\mathbf{n},i} \Gamma_{\mathbf{n},i} c^{\alpha\dagger}_{\mathbf{n}} \sigma_i^{\alpha\beta} c^{\beta}_{\mathbf{n}+\mathbf{a}_i} + \text{H.c.}, \tag{A1}$$

where the hopping integral $\Gamma_{\mathbf{n},i}$ becomes

$$\Gamma_{\mathbf{n},i} = \gamma \exp\left\{ i\frac{ea}{c\hbar}\int_{s=0}^{1} A_i(\mathbf{n}+s\mathbf{a}_i,t)\right\}. \tag{A2}$$

Applying the charge symmetry transformation $c^{\alpha}_{\mathbf{n}} \to e^{i\chi_{\mathbf{n}}(t)} c^{\alpha}_{\mathbf{n}}$, the current density on the link is

$$J_{\mathbf{n}i}(t) \equiv -\frac{c}{\mathcal{V}}\frac{\delta}{\delta A_{\mathbf{n}i}(t)}\widehat{K}_{mc}. \tag{A3}$$

In linear response the current density operator is expanded up to the first order in $A_{\mathbf{n}i}$ as $J_{\mathbf{n}i}(t) = J^{p}_{\mathbf{n}i}(t) + J^{d}_{\mathbf{n}i}(t)$:

$$\begin{aligned} J^{p}_{\mathbf{n}i}(t) &= \frac{ev}{2\mathcal{V}} c^{\alpha\dagger}_{\mathbf{n}} \sigma_i^{\alpha\beta} c^{\beta}_{\mathbf{n}+\mathbf{a}_i} + \text{H.c.}, \\ J^{d}_{\mathbf{n}i}(t) &= i\frac{e^2 va}{2c\hbar\mathcal{V}}\int_{s=0}^{1} A_i(\mathbf{n}+s\mathbf{a}_i,t) c^{\alpha\dagger}_{\mathbf{n}} \sigma_i^{\alpha\beta} c^{\beta}_{\mathbf{n}+\mathbf{a}_i} + \text{H.c.} \end{aligned} \tag{A4}$$

Normalized operators in momentum space are $c^{\alpha}_{\mathbf{n}} = \mathcal{N}^{-1/2}\sum_{\mathbf{k}} e^{-i\mathbf{k}\cdot\mathbf{n}} c^{\alpha}_{\mathbf{k}}$, where the number of unit cells is $\mathcal{N} = \mathcal{V}/a^3$ with $\mathcal{V} = a^3\sum_{\mathbf{n}} 1$, where $\widehat{k}_i = \sin(ak_i)$. There are eight Weyl points at which $\varepsilon_{\mathbf{k}} \propto |\widehat{\mathbf{k}}| = 0$ inside the Brillouin zone. The calculation therefore was performed for $N = 8$.

2. Matsubara action and Feynman rules

It is useful to represent the electron gas via the Matsubara action ($\tau = it$) involving the $3+1$ fermion field ψ and the static photon (auxiliary) field ϕ. Using convenient units with $a = \gamma = \hbar = 1$, it reads

$$A = \sum_{\mathbf{n}}\int_{\tau}\left\{\begin{array}{l} \psi^{\dagger}_{\mathbf{n}}(\tau)\left(\frac{d}{d\tau} - ie\phi_{\mathbf{n}}\right)\psi_{\mathbf{n}}(\tau) - \frac{1}{2}\sum_i (\psi^{\dagger}_{\mathbf{n}}(\tau)\sigma_i\psi_{\mathbf{n}+\mathbf{a}_i}(\tau) + \text{H.c.}) \\ \quad + \frac{1}{2}\sum_i \left[2\phi_{\mathbf{n}}(\tau) - \phi_{\mathbf{n}+\mathbf{a}_i}(\tau) - \phi_{\mathbf{n}-\mathbf{a}_i}(\tau)\right]\phi_{\mathbf{n}}(\tau) \end{array}\right\}. \tag{A5}$$

The Feynman rules can be read from the Fourier transform

$$\begin{aligned} A = \sum_{\mathbf{k}\omega}\left\{\psi^{\dagger}_{\mathbf{k}\omega}(i\omega - \widehat{\mathbf{k}}\cdot\sigma)\psi_{\mathbf{k}\omega} - ie\sum_{\mathbf{p}\nu}\psi^{\dagger}_{\mathbf{k}\omega}\psi_{\mathbf{k}-\mathbf{p},\omega-\nu}\phi_{\mathbf{p}\nu}\right\} \\ + \frac{1}{2}\sum_{\mathbf{p}\nu i}\phi^{*}_{\mathbf{p}\nu}[1-\cos(p_i)]\phi_{\mathbf{p}\nu}. \end{aligned} \tag{A6}$$

The fermion propagator is

$$G_{\mathbf{p}\omega} = (i\omega - \widehat{\mathbf{p}}\cdot\sigma)^{-1} = \frac{-i\omega - \widehat{\mathbf{p}}\cdot\sigma}{\omega^2 + \varepsilon^2_{\mathbf{p}}}, \tag{A7}$$

while the photon propagator is frequency independent, $g_{\mathbf{p}\omega} = v_{\mathbf{p}}$. The vertex is $ie\delta_{\mathbf{k}-\mathbf{k}'+\mathbf{p}}\delta_{\omega-\omega'}$. These Feynman rules are used to calculate the linear response diagramatically.

APPENDIX B: DIRECT CALCULATION OF THE CONDUCTIVITY TENSOR FOR THE NONINTERACTING WSM

1. General relation between the conductivity tensor and the dielectric constant

We calculate the transversal and longitudinal conductivities $\sigma_{\rm T}$ and $\sigma_{\rm L}$. From Eq. (3) we derive an expression for two scalars formed from the conductivity tensor σ_{ij}:

$$\begin{aligned} 2\sigma_{\rm T}(\omega,k)+\sigma_{\rm L}(\omega,k)&=\sigma_{ii}(\omega),\\ \sigma_{\rm L}(\omega,k)&=\lim_{k\to 0}\frac{k_ik_j}{k^2}\sigma_{ij}(\omega). \end{aligned} \tag{B1}$$

Of course, due to charge conservation the transverse conductivity is proportional to the dielectric constant (Matsubara) [1]

$$\sigma_{\rm L}(\omega,k)=\frac{\omega}{4\pi}[1-\varepsilon_{\rm L}(\omega,k)]. \tag{B2}$$

2. The noninteracting WSM

The ac conductivity of the noninteracting WSM on the lattice is obtained from the Kubo formula. The trace is (for positive ω)

$$\begin{aligned} \sigma_{ii}(\omega)&=\frac{e^2}{\hbar v\omega}\sum_{\mathbf{p},\nu}{\rm Tr}\{\sigma_i G_{\mathbf{p},\nu}\sigma_i(G_{\mathbf{p},\nu+\omega}-G_{\mathbf{p},\nu})\}\\ &=2\frac{e^2}{\hbar v}\sum_{\mathbf{p}}\frac{\omega}{\varepsilon_{\mathbf{p}}\left(\omega^2+4\varepsilon_{\mathbf{p}}^2\right)}, \end{aligned} \tag{B3}$$

while the longitudinal conductivity is

$$\begin{aligned} \sigma_{\rm L}(\omega)&=\lim_{k\to 0}\frac{e^2}{\hbar v\omega k^2}\sum_{\mathbf{p},\nu}{\rm Tr}\{\mathbf{k}\cdot\sigma G_{\mathbf{p},\nu}\mathbf{k}\cdot\sigma(G_{\mathbf{p},\nu+\omega}-G_{\mathbf{p},\nu})\}\\ &=\frac{2}{3}\frac{e^2}{\hbar v}\sum_{\mathbf{p}}\frac{\omega}{\varepsilon_{\mathbf{p}}\left(\omega^2+4\varepsilon_{\mathbf{p}}^2\right)}=\frac{1}{3}\sigma_{ii}. \end{aligned} \tag{B4}$$

From here one deduces that $\sigma_{\rm T}=\sigma_{\rm L}$ and thus no nonlocal conductivity arises in the noninteracting relativistic system (see general arguments in [27]).

On the lattice one obtains (unit of length $a=\hbar=v=1$)

$$\sigma_{\rm T}^{(0)}=\sigma_{\rm L}^{(0)}=\sigma_0=\frac{e^2\omega}{3\pi^2}\log\frac{\Omega^2}{\omega^2}; \tag{B5}$$

$\Omega\simeq 2.5\pi v/a$ is the ultraviolet frequency cutoff. This result is consistent with [20]. The (Matsubara) dielectric constant to this order is

$$\varepsilon=1-\frac{4e^2}{3\pi}\log\frac{\Omega^2}{\omega^2}. \tag{B6}$$

Generalizing the results from our particular model with eight Weyl fermions to arbitrary number N of the Weyl fermionic fields by just multiplication by $N/8$ (and in physical units), one gets

$$\sigma_0=\frac{e^2N\omega}{24\pi^2v\hbar}\log\frac{\Omega^2}{\omega^2}. \tag{B7}$$

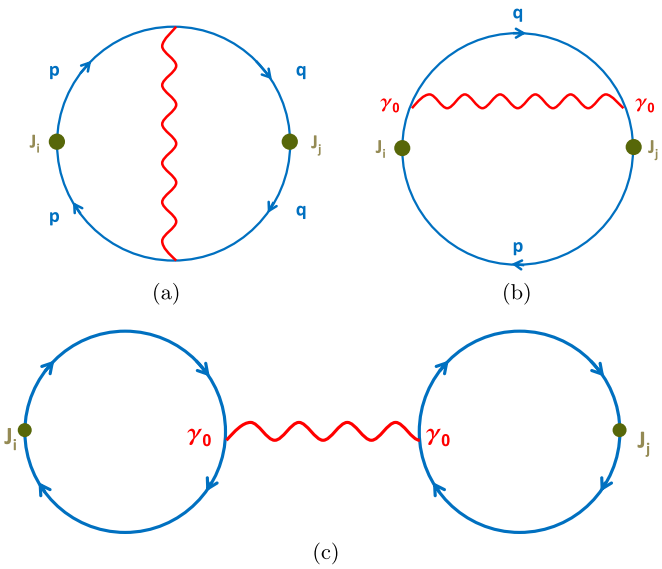

FIG. 6. The Feynman diagrams for conductivity tensor. (a) The vertex correction. (b) The self-energy correction. (c) The glasses correction.

The continuation to physical frequencies ($\omega_M\to -i\omega$) gives

$$\sigma_0=\frac{e^2N\omega}{24\pi v\hbar}\left(1-\frac{i}{\pi}\log\frac{\Omega^2}{\omega^2}\right). \tag{B8}$$

APPENDIX C: THE INTERACTION CORRECTIONS

1. Calculation of the trace of the conductivity tensor, Eq. (B1)

The three interaction corrections to the trace of the conductivity tensor are the self-energy, the vertex, and the "glasses" corrections [see Figs. 6(a)–6(c)] $\sigma_{ii}^{(1)}=e^2\alpha(\sigma_{ii}^{\rm ver}+\sigma_{ii}^{\rm se}+\sigma_{ii}^{\rm gl})$,

$$\begin{aligned} \sigma_{ii}^{\rm ver}&=\frac{1}{\omega}\sum_{\mathbf{pq}\nu\rho}{\rm Tr}[v_{\mathbf{q}-\mathbf{p}}\,\widetilde{\mathbf{p}}\cdot\widetilde{\mathbf{q}}\,G_{\mathbf{p},\nu}G_{\mathbf{q},\rho}\sigma_iG_{\mathbf{q},\rho+\omega}G_{\mathbf{p},\omega+\nu}\sigma_i\\ &\quad-\{\omega\to 0\}];\\ \sigma_{ii}^{\rm se}&=-\frac{2}{\omega}\sum_{\mathbf{pq}\nu\rho}{\rm Tr}[v_{\mathbf{q}-\mathbf{p}}\widetilde{\mathbf{p}}\cdot\widetilde{\mathbf{p}}\,G_{\mathbf{p},\nu}G_{\mathbf{q},\rho}G_{\mathbf{p},\nu}\sigma_iG_{\mathbf{p},\omega+\nu}\sigma_i];\\ \sigma_{ii}^{\rm gl}&=\frac{1}{\omega}v_{\mathbf{k}}\left(\sum_{\mathbf{p},\nu}{\rm Tr}G_{\mathbf{p},\nu}G_{\mathbf{k}+\mathbf{p},\omega+\nu}\right)^2, \end{aligned} \tag{C1}$$

where the first term is the vertex, the second term the self-energy, and the third term the glasses diagram. The following shorthand is useful:

$$\begin{aligned} &\widehat{k}_i\equiv\sin k_i;\ \widetilde{k}_i\equiv\cos(k_i);\ \widehat{2k}_i\equiv\sin(2k_i);\varepsilon_k=\sqrt{\widehat{\mathbf{k}}^2};\\ &\widehat{\mathbf{k}}^n=\left\{\widehat{k}_1^{\,n},\widehat{k}_2^{\,n},\widehat{k}_3^{\,n}\right\},\quad \widetilde{\mathbf{k}}^n=\left\{\widetilde{k}_1^{\,n},\widetilde{k}_2^{\,n},\widetilde{k}_3^{\,n}\right\}. \end{aligned} \tag{C2}$$

Calculating the trace and integrating over the internal frequencies ν and ρ results in the following expressions for the three diagrams (symmetrized in $\mathbf{p}$ and $\mathbf{q}$). The vertex

$$\sigma_{ii}^{\rm ver}=\frac{1}{\omega}\frac{1}{36}\sum_{\mathbf{qp}}\frac{v_{\mathbf{q}-\mathbf{p}}(\Xi_1+\Xi_2)}{\varepsilon_{\mathbf{p}}\varepsilon_{\mathbf{q}}\left(\omega^2+4\varepsilon_{\mathbf{p}}^2\right)^2\left(\omega^2+4\varepsilon_{\mathbf{q}}^2\right)^2}, \tag{C3}$$

with

$$\Xi_1 = -\omega^2\{4\,(\widehat{\mathbf{p}}\cdot\widehat{\mathbf{q}})\,(\widetilde{\mathbf{p}}\cdot\widetilde{\mathbf{q}}) - \widehat{\mathbf{2p}}\cdot\widehat{\mathbf{2q}}\};$$
$$\Xi_2 = 2\Big\{\begin{array}{l}(\widehat{\mathbf{p}}\cdot\widehat{\mathbf{q}})\,(\widehat{\mathbf{2p}}\cdot\widehat{\mathbf{2q}}) + 12\widetilde{\mathbf{p}}\cdot\widetilde{\mathbf{q}} - 16\varepsilon_{\mathbf{p}}^2\,\widetilde{\mathbf{p}}\cdot\widetilde{\mathbf{q}} + 24\widetilde{\mathbf{q}}^3\cdot\widetilde{\mathbf{p}} \\ \quad + 4(\widetilde{\mathbf{p}}\cdot\widetilde{\mathbf{p}})\,(\widetilde{\mathbf{q}}\cdot\widetilde{\mathbf{q}})(\,\widetilde{\mathbf{p}}\cdot\widetilde{\mathbf{q}}) - 8(\widetilde{\mathbf{p}}\cdot\widetilde{\mathbf{p}})\,(\widetilde{\mathbf{q}}^3\cdot\widetilde{\mathbf{p}}) + \mathbf{p}\longleftrightarrow\mathbf{q}\end{array}\Big\},$$

the self-energy,

$$\sigma_{ii}^{\rm se} = -\frac{1}{\omega}\frac{1}{3}\sum_{\mathbf{qp}}\frac{v_{\mathbf{q}-\mathbf{p}}}{\varepsilon_p\varepsilon_q}\left(\frac{\Xi_3+\Xi_4}{\varepsilon_p^2\left(\omega^2+4\varepsilon_p^2\right)^2}+\mathbf{p}\longleftrightarrow\mathbf{q}\right), \tag{C4}$$

$$\Xi_3 = \omega^2\left\{-\varepsilon_p^4(\widehat{\mathbf{p}}\cdot\widehat{\mathbf{q}}) + 2\varepsilon_p^2(\widehat{\mathbf{p}}^3\cdot\widehat{\mathbf{q}}) + 2\varepsilon_p^2(\widehat{\mathbf{p}}\cdot\widehat{\mathbf{q}}) - (\widehat{\mathbf{p}}^2\cdot\widehat{\mathbf{p}}^2)(\widehat{\mathbf{p}}\cdot\widehat{\mathbf{q}})\right\};$$
$$\Xi_4 = 4\varepsilon_p^2\left\{\varepsilon_p^4(\widehat{\mathbf{p}}\cdot\widehat{\mathbf{q}}) + 2\varepsilon_p^2(\widehat{\mathbf{p}}^3\cdot\widehat{\mathbf{q}}) - 2\varepsilon_p^2(\widehat{\mathbf{p}}\cdot\widehat{\mathbf{q}}) - 3(\widehat{\mathbf{p}}^2\cdot\widehat{\mathbf{p}}^2)(\widehat{\mathbf{p}}\cdot\widehat{\mathbf{q}})\right\},$$

and the glasses diagram that is proportional to the square of the number of the Weyl points. Generalizing to arbitrary number N of Weyl points, one has

$$\sigma_{ii}^{\rm gl} = \frac{e^4}{\omega}\frac{4\pi N^2}{3}\left(\sum_p\frac{\widehat{p}_y^2\widetilde{p}_x}{\varepsilon_{\mathbf{p}}^3\left(\omega^2+4\varepsilon_{\mathbf{p}}^2\right)}\right)^2. \tag{C5}$$

The integration over the momenta is performed with the sum of the vertex and the self-energy diagrams, which ensures convergence. The integral for the glasses diagram vanishes. The result is

$$\sigma_{ii}^{(1)} = \frac{N\alpha^2\omega}{24\pi}\left(3.053+\frac{1.036}{\pi}\log(\omega^2)+\frac{1}{2\pi^2}\log^2(\omega^2)\right). \tag{C6}$$

2. The longitudinal conductivity via the dielectric constant, Eq. (B2)

The general expressions for the dielectric function (the longitudinal part) via the $\rho-\rho$ correlator can be written as $\varepsilon_{\rm L} = 1 + e^2\varepsilon_{\rm L}^{(0)} + e^2\alpha\varepsilon_{\rm L}^{(1)}$ with

$$\varepsilon^{(0)} = -v_{\mathbf{k}}{\rm Tr}\sum_{\mathbf{p}\nu}G_{\mathbf{p},\nu}G_{\mathbf{p}+\mathbf{k},\nu+\omega}, \tag{C7}$$

and $\varepsilon_{\rm L}^{(1)} = \varepsilon^{\rm ver} + \varepsilon^{\rm se} + \varepsilon^{\rm gl}$, where

$$\begin{aligned}\varepsilon^{\rm ver} &= v_{\mathbf{k}}\sum_{\mathbf{pq}\nu\rho}{\rm Tr}G_{\mathbf{p}+\mathbf{k},\nu+\omega}G_{\mathbf{p},\nu}v_{\mathbf{q}}G_{\mathbf{p}+\mathbf{q},\rho}G_{\mathbf{p}+\mathbf{q}+\mathbf{k},\rho+\omega};\\ \varepsilon^{\rm se} &= -2v_{\mathbf{k}}\sum_{\mathbf{pq}\nu\rho}v_{\mathbf{q}-\mathbf{p}}{\rm Tr}G_{\mathbf{p},\nu}G_{\mathbf{q},\rho}G_{\mathbf{p},\nu}G_{\mathbf{p}+\mathbf{k},\omega+\nu};\\ \varepsilon^{\rm gl} &= \left(v_{\mathbf{k}}{\rm Tr}\sum_{\mathbf{p}\nu}G_{\mathbf{p},\nu}G_{\mathbf{p}+\mathbf{k},\omega+\nu}\right)^2.\end{aligned} \tag{C8}$$

The sums are expanded in powers of k; the trace is calculated and integrated over the internal frequencies. All the terms divergent in the $k\to 0$ limit vanish after integration over the internal frequencies. The relevant terms (symmetrized in $\mathbf{p}$ and $\mathbf{q}$) at $k=0$ are

$$\varepsilon^{\rm se} = \frac{\pi}{6}\sum_{\mathbf{qp}}\frac{v_{\mathbf{q}-\mathbf{p}}}{\varepsilon_{\mathbf{p}}\varepsilon_{\mathbf{q}}}\left\{\begin{array}{c}\left(\frac{\left(3-\varepsilon_{\mathbf{p}}^2\right)\left(\omega^2-4\varepsilon_{\mathbf{p}}^2\right)+2\left(\omega^2+12\varepsilon_{\mathbf{p}}^2\right)}{2\left(\omega^2+4\varepsilon_{\mathbf{p}}^2\right)^2\varepsilon_{\mathbf{p}}^2}-\frac{\left[3\omega^2+20\varepsilon_{\mathbf{p}}^2\right](\widehat{\mathbf{2p}})^2}{8\varepsilon_{\mathbf{p}}^4\left(\omega^2+4\varepsilon_{\mathbf{p}}^2\right)^2}\right)\widehat{\mathbf{p}}\cdot\widehat{\mathbf{q}}\\ -\frac{\left(\omega^2+12\varepsilon_{\mathbf{p}}^2\right)\widehat{\mathbf{p}}^3\cdot\widehat{\mathbf{q}}}{\left(\omega^2+4\varepsilon_{\mathbf{p}}^2\right)^2\varepsilon_{\mathbf{p}}^2}\end{array}\right\}+\mathbf{p}\longleftrightarrow\mathbf{q}; \tag{C9}$$

$$\varepsilon^{\rm ver} = \frac{\pi}{6}\sum_{\mathbf{qp}}\frac{v_{\mathbf{q}-\mathbf{p}}}{\varepsilon_{\mathbf{p}}^3\varepsilon_{\mathbf{q}}^3\left(\omega^2+4\varepsilon_{\mathbf{p}}^2\right)\left(\omega^2+4\varepsilon_{\mathbf{q}}^2\right)}\left\{\begin{array}{l}\left[4\varepsilon_{\mathbf{p}}^2\varepsilon_{\mathbf{q}}^2-\omega^2(\widehat{\mathbf{p}}\cdot\widehat{\mathbf{q}})\right](\widehat{\mathbf{2p}}\cdot\widehat{\mathbf{2q}})\\ \quad+4\varepsilon_{\mathbf{p}}^2\varepsilon_{\mathbf{q}}^2[4(\widehat{\mathbf{p}}\cdot\widehat{\mathbf{q}})-\omega^2](\widetilde{\mathbf{p}}\cdot\widetilde{\mathbf{q}})\\ \quad-2\varepsilon_{\mathbf{p}}^2\left\{2\varepsilon_{\mathbf{q}}^2(\widehat{\mathbf{2p}}\cdot\widehat{\mathbf{2q}})-\omega^2\widehat{2\mathbf{q}}\cdot(\widehat{\mathbf{q}}*\widetilde{\mathbf{p}})\right\}\end{array}\right\}+\mathbf{p}\longleftrightarrow\mathbf{q}; \tag{C10}$$

$$\varepsilon^{\rm gl} = \frac{\pi^2}{4}\left\{\sum_{\mathbf{p}} \frac{\frac{1}{3}(\widehat{\mathbf{p}}^2\cdot\widehat{\mathbf{p}}^2)+\frac{1}{12}\widehat{\mathbf{2p}}^2-\varepsilon_{\mathbf{p}}^2}{\varepsilon_{\mathbf{p}}^3\left(\omega^2+4\varepsilon_{\mathbf{p}}^2\right)}\right\}^2. \tag{C11}$$

The numerical integration over the internal momenta results in, generalizing to N Weyl fermions,

$$\begin{aligned}\varepsilon_{\rm L}^{\rm se+ver} &= -Ne^2\alpha\left\{0.091+\frac{0.146}{6\pi}\log\omega^2+\frac{1}{36\pi^2}\log^2(\omega^2)\right\};\\ \varepsilon_{\rm L}^{\rm gl} &= N^2e^2\alpha\left\{0.22-\frac{1}{6\pi}\log(\omega^2)\right\}^2.\end{aligned} \tag{C12}$$

The longitudinal conductivity correction thus is

$$\sigma_{\rm L}^{(1)} = -\frac{\omega}{4\pi}\varepsilon_{\rm L}^{(1)} = \frac{Ne^2\alpha\omega}{24\pi}\left\{0.545+\frac{0.146}{\pi}\log\omega^2+\frac{1}{6\pi^2}\log^2(\omega^2)-6N\left(0.22-\frac{1}{6\pi}\log(\omega^2)\right)^2\right\}. \tag{C13}$$

3. Nonlocal conductivity: Analytic continuation to physical frequency

Using the expressions for the conductivity tensor trace and $\sigma_{\rm L}$ given in Eqs. (C6) and (C13), one obtains the corrections to transversal and nonlocal conductivities

$$\sigma_{\rm nl} = \sigma_{\rm L}-\sigma_{\rm T} = \frac{1}{2}\left(3\sigma_{\rm L}^{(1)}-\sigma_{ii}^{(1)}\right) = \frac{e^2\alpha\omega}{24\pi}\left\{N\left(-0.71-\frac{1}{\pi^2}\log(\omega^2)\right)-9N^2\left(0.22-\frac{1}{6\pi}\log(\omega^2)\right)^2\right\}. \tag{C14}$$

Continuation to physical frequencies ($\omega_M \to -i\omega$) results in the following real and imaginary parts (in terms of the ultraviolet cutoff frequency Ω):

$$\begin{aligned}\sigma_{\rm nl}' &= \frac{Ne^2\alpha\omega}{24\pi^2}\left\{1+\frac{N}{2}\log\frac{\Omega^2}{\omega^2}\right\};\\ \sigma_{\rm nl}'' &= \frac{Ne^2\alpha\omega}{24\pi^2}\left\{\left(\frac{\pi}{4}N-2.23\right)+\frac{1}{\pi}\log\frac{\Omega^2}{\omega^2}-\frac{N}{4\pi}\log^2\frac{\Omega^2}{\omega^2}\right\}.\end{aligned} \tag{C15}$$

One observes that the contribution of the real part of the nonlocal conductivity is positive for frequencies up to $\Omega/e^{1/N}$, while the sign of the the imaginary part can depend on frequency and N. It is negative at small frequencies and large N. The Nielsen-Ninomiya theorem ensures $N \geqslant 4$ in 3D.

APPENDIX D: FERMI ARCS

Absence of edge states along the [100] cut

Annihilation operators in "half momentum half configuration" space, $c^{\alpha}_{n_x n_y n_z} = \sum_{k_y,k_z} e^{-i(k_y n_y + k_z n_z)} c^{\alpha}_{n_x k_y k_z}$, are useful to this end since the boundary maintains the translation symmetry of the bulk in the y,z directions. Using the tight-binding Hamiltonian takes a form of the sum of one-dimensional operators, $K = \sum_{k_y,k_z} K_{k_\perp}$,

$$K_{k_\perp} = \frac{iv}{2}\sum_{n_x=1} c^{\dagger}_{n_x,k_\perp}\left[(e^{-ik_y a}\sigma_{yx}+e^{-ik_z a}\sigma_z)c_{n_z,k_\perp} + \sigma_x c_{n_z+1,k_\perp}\right] + \text{H.c.} \tag{D1}$$

To simplify notations, we denote $k_\perp \to k$, $n_x \to n$ and taking $a = 1$. The Schrödinger equation away from the surface ($n > 1$) is

$$(\hat{k}_y\sigma_y+\hat{k}_z\sigma_z)\psi_n + \frac{i}{2}\sigma_x(\psi_{n+1}-\psi_{n-1}) = 0, \tag{D2}$$

where $\hat{k} \equiv \sin(k)$

The edge states would correspond to solutions of the type $\psi_{n+1} = \lambda\psi_n = \lambda^n\psi_1$. The projection matrix

$$P = (\hat{k}_y\sigma_y+\hat{k}_z\sigma_z)+\frac{i}{2}(\lambda-\lambda^{-1})\sigma_x \tag{D3}$$

does not allow the nontrivial solutions.

APPENDIX E: TRANSVERSAL AND LONGITUDINAL WAVES PROPAGATION IN THE BULK OF WSM

1. The transversal wave dispersion

The dispersion relation, Eq. (12), with the bulk conductivity including the p^2 term,

$$\sigma_{\rm T} = \frac{Ne^2\omega}{24\pi}\left(1-i\frac{1}{\pi}\log\frac{\Omega^2}{\omega^2}\right)\left(1-\frac{v^2p^2}{\omega^2}\right), \tag{E1}$$

takes a form

$$\frac{c^2}{\omega^2}p^2 = 1+i\frac{N}{6}\left(1-i\frac{1}{\pi}\log\frac{\Omega^2}{\omega^2}\right)\left(1-\frac{v^2}{\omega^2}p^2\right). \tag{E2}$$

Its solution is

$$p^2 = \frac{\omega^2}{c^2}\frac{1 + i\frac{N}{6}\left(1 - i\frac{1}{\pi}\log\frac{\Omega^2}{\omega^2}\right)}{1 + i\frac{N}{6}\left(1 - i\frac{1}{\pi}\log\frac{\Omega^2}{\omega^2}\right)\frac{v^2}{c^2}}. \tag{E3}$$

Since $v/c \ll 1$, one obtains

$$p^2 = \frac{\omega^2}{c^2}\left[1 + i\frac{N}{6}\left(1 - i\frac{1}{\pi}\log\frac{\Omega^2}{\omega^2}\right)\right] \tag{E4}$$

so that

$$\begin{aligned} p &= \pm\frac{\omega}{c}\sqrt{1 + \frac{N}{6\pi}\log\frac{\Omega^2}{\omega^2} + i\frac{N}{6}} \\ &\simeq \pm\frac{\omega}{c}\sqrt{1 + \frac{N}{6\pi}\log\frac{\Omega^2}{\omega^2}}\left(1 + i\frac{N}{12\left(1 + \frac{N}{6\pi}\log\frac{\Omega^2}{\omega^2}\right)}\right). \end{aligned} \tag{E5}$$

The last expression utilizes $\frac{1}{\pi}\log\frac{\Omega^2}{\omega^2} \gg 1$. Consequently, to the leading order the dispersion relation is real

$$p = \pm\frac{\omega}{c}\sqrt{1 + \frac{Ne^2}{6\pi}\log\frac{\Omega^2}{\omega^2}}, \tag{E6}$$

while the penetration depth is

$$\delta_{\mathrm{T}} = \frac{1}{\mathrm{Im}p} = \frac{c}{\omega}\frac{12}{Ne^2}\sqrt{1 + \frac{Ne^2}{6\pi}\log\frac{\Omega^2}{\omega^2}}. \tag{E7}$$

2. The longitudinal wave dispersion

The main contribution to the longitudinal conductivity $\sigma_{\mathrm{L}}(\omega)$ comes from the imaginary part, so that the dispersion relation, Eq. (13), for plasmons becomes

$$q = \frac{\omega}{v}\sqrt{\frac{1 + \frac{Ne^2}{6\pi}\left(1 - \frac{\alpha}{\pi}\right)\log\frac{\Omega^2}{\omega^2} - \frac{e^2\alpha N^2}{24\pi^2}\log^2\left(\frac{\Omega^2}{\omega^2}\right)}{\frac{Ne^2}{6\pi}\left(\log\frac{\Omega^2}{\omega^2} - 1\right)}}, \tag{E8}$$

and the penetration depth is

$$\delta_{\mathrm{L}} = \frac{v}{\omega}\sqrt{\frac{4\pi}{N\alpha}\log\frac{\Omega^2}{\omega^2}} = \frac{v^2}{\omega^2}\frac{4\pi}{N\alpha}q. \tag{E9}$$

[1] G. Giuliani and G. Vignale, *Quantum Theory of the Electron Liquid* (Cambridge University Press, Cambridge, 2005).
[2] B. Rosenstein, H. C. Kao, and M. Lewkowicz, Phys. Rev. B **90**, 045137 (2014).
[3] P. A. Wolff, J. Phys. Chem. Solids **25**, 1057 (1964).
[4] X. Wan, A. M. Turner, A. Vishwanath, and S. Y. Savrasov, Phys. Rev. B **83**, 205101 (2011).
[5] G. Xu, H. Weng, Z. Wang, X. Dai, and Z. Fang, Phys. Rev. Lett. **107**, 186806 (2011).
[6] Z. K. Liu, B. Zhou, Y. Zhang, Z. J. Wang, H. M. Weng, D. Prabhakaran, S. K. Mo, Z. X. Shen, Z. Fang, X. Dai, Z. Hussain, and Y. L. Chen, Science **343**, 864 (2014).
[7] S. K. Kushwaha, J. W. Krizan, B. E. Feldman, A. Gyenis, M. T. Randeria, J. Xiong, S.-Y. Xu, N. Alidoust, I. Belopolski, T, Liang, M. Z. Hasan, N. P. Ong, A. Yazdani, and R. J. Cava, APL Mater. **3**, 041504 (2015).
[8] Z. Wang, Y. Sun, X.-Q. Chen, C. Franchini, G. Xu, H. Weng, X. Dai, and Z. Fang, Phys. Rev. B **85**, 195320 (2012).
[9] Z. K. Liu, J. Jiang, B. Zhou, Z. J. Wang, Y. Zhang, H. M. Weng, D. Prabhakaran, S.-K. Mo, H. Peng, P. Dudin, T. Kim, M. Hoesch, Z. Fang, X. Dai, Z. X. Shen, D. L. Feng, Z. Hussain, and Y. L. Chen, Nat. Mater. **13**, 677 (2014).
[10] Z. Wang, H. Weng, Q. Wu, X. Dai, and Z. Fang, Phys. Rev. B **88**, 125427 (2013).
[11] M. Neupane, S.-Y. Xu, R. Sankar, N. Alidoust, G. Bian, C. Liu, I. Belopolski, T.-R. Chang, H.-T. Jeng, H. Lin, A. Bansil, F. Chou, and M. Z. Hasan, Nat. Commun. **05**, 3786 (2014).
[12] M. Orlita, D. M. Basko, M. S. Zholudev, F. Teppe, W. Knap, V. I. Gavrilenko, N. N. Mikhailov, S. A. Dvoretskii, P. Neugebauer, C. Faugeras, A.-L. Barra, G. Martinez, and M. Potemski, Nat. Phys. **10**, 233 (2014).
[13] B. Q. Lv, H. M. Weng, B. B. Fu, X. P. Wang, H. Miao, J. Ma, P. Richard, X. C. Huang, L. X. Zhao, G. F. Chen, Z. Fang, X. Dai, T. Qian, and H. Ding, Phys. Rev. X **5**, 031013 (2015).
[14] B. Q. Lv, N. Xu, H. M. Weng, J. Z. Ma, P. Richard, X. C. Huang, L. X. Zhao, G. F. Chen, C. E. Matt, F. Bisti, V. N. Strocov, J. Mesot, Z. Fang, X. Dai, T. Qian, M. Shiand, and H. Ding, Nat. Phys. **11**, 724 (2015).
[15] S.-Y. Xu, N. Alidoust, I. Belopolski, Z. Yuan, G. Bian, T.-R. Chang, H. Zheng, V. N. Strocov, D. S. Sanchez, G. Chang *et al.*, Nat. Phys. **11**, 748 (2015).
[16] S.-Y. Xu, N. Alidoust, I. Belopolski, Z. Yuan, G. Bian, T.-R. Chang, H. Zheng, V. N. Strocov, D. S. Sanchez, G. Chang *et al.*, Science **349**, 613 (2015).
[17] T. Kariyado and M. Ogata, J. Phys. Soc. Jpn. **80**, 083704 (2011).
[18] T. Kariyado and Ogata, J. Phys. Soc. Jpn. **81**, 064701 (2012).
[19] J. Xiong, S. Kushwaha, J. Krizan, T. Liang, R. J. Cava, and N. P. Ong, Europhys. Lett. **114**, 27002 (2016).
[20] T. Liang, Q. Gibson, M. N. Ali, M. Liu, R. J. Cava, and N. P. Ong, Nat. Mater. **14**, 280 (2015).
[21] H. Wang, H. Wang, H. Liu, H. Lu, W. Yang, S. Jia, X.-J. Liu, X. C. Xie, J. Wei, and J. Wang, Nat. Mater. **15**, 38 (2016).
[22] B. Rosenstein and M. Lewkowicz, Phys. Rev. B **88**, 045108 (2013).
[23] M. Lv and S. C. Zhang, Int. J. Mod. Phys. B **27**, 1250177 (2013).
[24] P. Hosur, S. A. Parameswaran, and A. Vishwanath, Phys. Rev. Lett. **108**, 046602 (2012).
[25] R. E. Throckmorton, J. Hofmann, E. Barnes, and S. Das Sarma, Phys. Rev. B **92**, 115101 (2015).
[26] B. Rosenstein, M. Lewkowicz, and T. Maniv, Phys. Rev. Lett. **110**, 066602 (2013).
[27] V. Mastropietro, J. Phys. A **47**, 465003 (2014).
[28] K. Ziegler, Eur. Phys. J. B **89**, 268 (2016).
[29] A. G. Grushin, J. W. F. Venderbos, and J. H. Bardarson, Phys. Rev. B **91**, 121109(R) (2015).
[30] L. D. Landau, E. M. Lifshitz, and L. P. Pitaevskii, *Electrodynamics of Continuous Media* (Elsevier Butterworth-Heinemann, Oxford, 1984).

[31] A. A. Golubkov and V. A. Makarov, Phys. Usp. **38**, 325 (1995).
[32] V. M. Agranovich and V. L. Ginzburg, *Crystal Optics with Spatial Dispersion, and Excitons* (Springer-Verlag, Berlin, 1984).
[33] S. I. Pekar, Sov. Phys. JETP **6**, 785 (1958).
[34] M. Born, E. Wolf, and A. B. Bhatia, *Principles of Optics* (Cambridge University Press, Cambridge, UK, 1999).
[35] S. A. Parameswaran, T. Grover, D. A. Abanin, D. A. Pesin, and A. Vishwanath, Phys. Rev. X **4**, 031035 (2014).
[36] A. C. Potter, I. Kimchi, and A. Vishwanath, Nat. Commun. **5**, 5161 (2014).
[37] J. Gonzalez, Phys. Rev. B **90**, 121107(R) (2014).
[38] H. Isobe and N. Nagaosa, Phys. Rev. B **87**, 205138 (2013).
[39] M. Zivitz and J. R. Stevenson, Phys. Rev. B **10**, 2457 (1974).
[40] J. P. Jay-Gerin, M. J. Aubin, and L. G. Caron, Solid State Commun. **21**, 771 (1977).
[41] E. Barnes, E. H. Hwang, R. E. Throckmorton, and S. Das Sarma, Phys. Rev. B **89**, 235431 (2014).
[42] D. A. Siegel, C.-H. Park, C. Hwang, J. Deslippe, A. V. Fedorov, S. G. Louie, and A. Lanzara, Proc. Natl. Acad. Sci. U.S.A. **108**, 11365 (2011).
[43] G. L. Yu, R. Jalil, B. Belle, A. S. Mayorov, P. Blake, F. Schedin, S. V. Morozov, L. A. Ponomarenko, F. Chiappini, S. Wiedmann, U. Zeitler, M. I. Katsnelson, A. K. Geim, K. S. Novoselov, and D. C. Elias, Proc. Natl. Acad. Sci. U.S.A. **110**, 3282 (2013).